29th Congress of the International Council of the Aeronautical Sciences
St. Petersburg, Russia; September 7-12, 2014

THEORETICAL MODELING OF THE ELECTROGASDYNAMIC METHOD OF LAMINAR FLOW CONTROL ON A SWEPT WING

Chernyshev S.L., Kuryachii A.P., Manuilovich S.V., Rusyanov D.A., Gamirullin M.D.
Central Aerohydrodynamic Institute, Zhukovsky, Russia

Keywords: *plasma actuators, cross-flow instability*

Abstract

Calculations of 3D compressible boundary layer on infinite span swept wing with volumetric force and heat impact of plasma actuators are executed. The linear stability of boundary layer flow with respect to stationary modes of the cross-flow-type disturbances is considered. The position of the laminar-turbulent transition is estimated with the aid of e^N-method. Assessments of actuators impact necessary for laminar-turbulent transition delay are obtained for free stream parameters corresponding to typical cruise flight conditions of subsonic civil airplane.

1 Introduction

A development of innovative aerodynamic technologies aimed on substantial reduction in fuel consumption and atmospheric pollution remains in the centre of attention of the aeronautical community, industry and research centers [1]. Cruise drag reduction promotes achievement this goal. The viscous drag contributes about a half of the total cruise drag of modern civil airplanes. A delaying laminar to turbulent boundary layer transition on aerodynamic surfaces is one of the effective methods of viscous drag reduction. The cross-flow-type instability is, as a rule, the main reason of laminar-turbulent transition on a swept wing [2]. Therefore any method of suppression of this instability would be a key to solution the problem of a swept wing drag reduction, if this method is energy acceptable.

The concept of laminar flow control (LFC) method proposed at TsAGI [3] and based on an attenuation of the cross-flow-type instability due to electrogasdynamic (EGD) force impact on three-dimensional boundary layer in the vicinity of a swept wing leading edge is illustrated in Fig. 1. The volumetric force impact of plasma actuators operating on the base of near-surface dielectric barrier discharge (DBD-actuators) [4-6] directed predominantly along a leading edge from a wing root to its tip will attenuate the cross-flow velocity and, as a consequence, decrease the increments of spatial growth of the cross-flow-type instability [7]. If this decrease is enough significant, the laminar-turbulent transition caused by the cross-flow-type instability can be delayed or wholly removed.

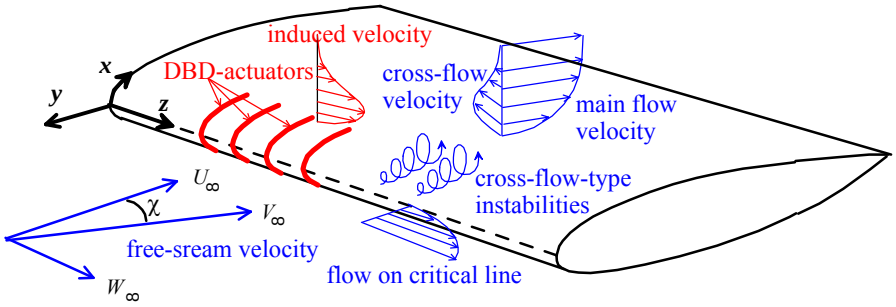

Fig. 1. The concept of the electrogasdynamic method of laminar flow control on a swept wing

Development and optimization of multiple DBD-actuators creating necessary force impact over significant part of a wing surface along a whole leading edge is a substantial problem for practical realization of EGD LFC method. The optimal design of DBD-actuators in series must ensure a discharge ignition only at one side of every exposed electrode and exclude it at the other side. Moreover main sizes of multi-actuator system such as the width of the exposed electrodes and the distance between them must be small enough in order to ensure a concentration of the volumetric force generated in DBD wholly inside a boundary layer with thickness less than 1 mm near the leading edge.

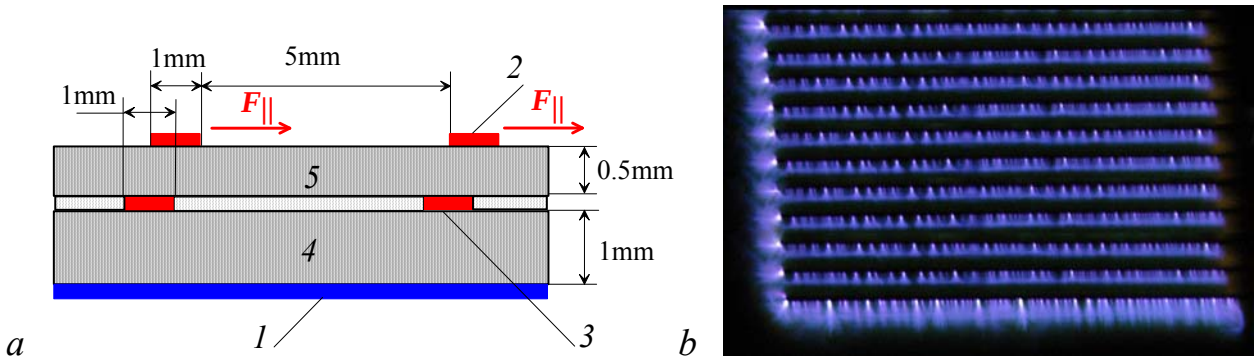

Fig. 2. The scheme of multiple DBD-actuator (*a*) and the picture of DBD on 11 actuators (*b*)

Simple design of multiple DBD-actuators proposed in [8] uses the concept of additional screening buried electrodes proposed in [9] but takes into account its assumed application on airplane wing and seems to be more effective. The scheme of the proposed system is shown in Fig. 2, *a* and consists of the continuous accelerating electrode common for all actuators in series (*1*), the narrow exposed electrodes (*2*), the narrow buried screening electrodes (*3*), two dielectric layers (*4*, *5*), and the glue layer between the dielectrics.

The metallic or composite electroconductive wing skin being under constant (zero) electric potential can be used as common accelerating electrode. The alternating electric potential is applied to the exposed and screening electrodes. The last prevent the discharge ignition near the left edges of the exposed electrodes. Therefore the average horizontal force $F_{||}$ generated by actuators accelerates gas flow from left to right over a whole surface.

The operability of the proposed system containing 11 DBD-actuators with the sizes in millimeters shown in Fig. 2, *a* is confirmed by Fig. 2, *b*. The amplitude and the frequency of the alternating voltage applied to the exposed and screening electrodes equal 8 kV and 10 kHz, respectively. It is seeing that the discharge fluorescence is observed only near one edge of every exposed electrode and gas accelerates top-down. The presented experimental results permit to use main geometric parameters of multi-actuator system similar to indicated in Fig. 2, *a* in the subsequent numerical modeling of actuators impact on boundary layer flow.

Experimental research and optimization of the EGD LFC method both in wind tunnels and flight tests is very expensive because of numerous geometrical and physical parameters governing this method. Therefore numerical simulation seems to be relevant for preliminary estimations of this method effectiveness. In the strict sense, numerical modeling of the dielectric barrier discharge actuators is necessary in order to calculate spatial distributions of volumetric force and energy release with subsequent their use in boundary layer calculations [10]. But such modeling even for one set of geometrical and physical parameters of DBD-actuator is very time consuming. Therefore analytical approximations for volumetric force and heat release predicted by phenomenological models of DBD are used, as a rule, in modeling of DBD impact on air flows [11]. This approach seems to be reasonable in preliminary parametric study of EGD LFC method.

2 Boundary layer calculations

Two variants of the arrangement of DBD-actuators on infinite span swept wing considered below are shown schematically in Fig. 3. Here the z-axis is directed along a critical line on the wing leading edge (see Fig. 1), the blue dashed curve in Fig. 3, *a* indicates the external inviscid streamline, the red solid lines denote the exposed electrodes of DBD-actuators arranged on a wing surface perpendicular to the leading edge in Fig. 3, *a* (variant *1*) or along the external streamline in Fig. 3, *b* (variant *2*) with the spatial period z_0 along a span. The red arrows show the directions of the volumetric force component $F_{||}$ parallel to a wing surface generated by actuators. The gas velocity vector at some point inside a boundary layer is denoted as V in Fig. 3, *a*, V_{CF} and V_{MF} are the cross-flow and main-flow components of V, u and w are the velocity components along the corresponding coordinates, the angle ψ in Fig. 3, *b* is formed by the external velocity vector V_e and the x-axis. The cross-flow and main-flow components of the boundary layer velocity according to Fig. 3 are determined as follows:

$$V_{CF}=u\sin\psi-w\cos\psi \qquad (1)$$

$$V_{MF}=u\cos\psi+w\sin\psi$$

$$\mathrm{tg}\psi=w_e/u_e,\ \ w_e=V_\infty\sin\chi$$

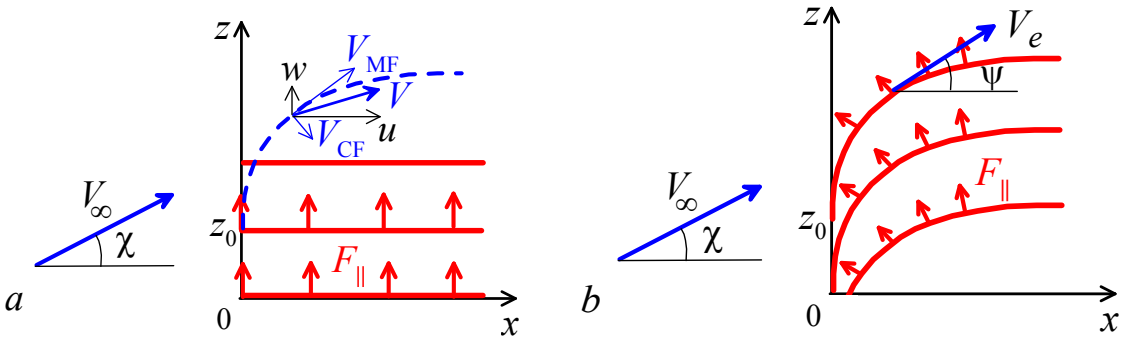

Fig. 3. Arrangements of multiple DBD-actuators on a wing surface: variant *1* (*a*), variant *2* (*b*)

The effect of DBD-actuators on cross-flow-type instability and laminar-turbulent transition is estimated by the example of flow over an infinite span swept wing with the sweep angle $\chi = 30^o$. The static pressure $p_\infty = 2.6\cdot10^4$ Pa, the air temperature $T_\infty = 223$ K corresponding to flight altitude about 10 km, and Mach number $M_\infty = 0.8$ are taken as the main free-stream parameters. They determine other flow parameters necessary for further boundary layer calculations: the flow velocity $V_\infty = 240$ m/s, the air density $\rho_\infty = 0.41$ kg/m^3, the dynamic viscosity coefficient $\mu_\infty = 1.33\cdot10^{-5}$ kg/(m·s).

The external boundary conditions for calculations of the compressible boundary layer have been obtained from the calculation of 2D inviscid flow over LV6 DLR airfoil at zero angle of attack on the base of the Euler equations. It is supposed that volumetric force and heat impact of plasma actuators is concentrated entirely inside a boundary layer. The spanwise modulation of the boundary layer displacement thickness resulting from actuators impact and corresponding viscous-inviscid interaction is not taken into consideration.

The boundary layer flow in the vicinity of a wing leading edge is characterized by Reynolds number $\mathrm{Re} = \rho_\infty V_\infty l/\mu_\infty$ determined by streamwise length $l = V_\infty/[du_e(0)/dx]$ (equals approximately a half radius of the leading edge curvature), where the x-coordinate is directed along a wing surface perpendicular to a leading edge, and u_e is the x-component of the external velocity obtained from inviscid calculation. The airfoil chord length normal to a leading edge L is related with the characteristic length l as $L = l\,du_e'(0)/dx'$, where the dimensionless velocity u_e' and the coordinate x' are measured in $V_\infty\cos\chi$ and L, respectively. According to executed 2D inviscid flow calculation, $du_e'(0)/dx' = 107.7$. The value $l = 0.03$ m is taken

in the present estimations, hence, the airfoil chord length equals $L = 3.23$ m. The specified above free-stream parameters and characteristic length l determine the value of the Reynolds number $\mathrm{Re} = 2.03 \cdot 10^5$ and the estimation for the boundary layer thickness near the critical line $\delta_0 \approx 5\mathrm{Re}^{-1/2} l \approx 0.33$ mm.

Calculated distributions of the non-dimensional x-component of the external flow velocity $u_e' = u_e / V_\infty$ and the streamwise pressure gradient $dp'/dx' = l/(\rho_\infty V_\infty^2)\, dp/dx$ in the vicinity of the wing leading edge are shown in Fig. 4. Zero angle of attack for a given airfoil has been taken in inviscid calculation because of a long enough part of streamwise flow acceleration and, as a consequence, intense cross-flow in the boundary layer.

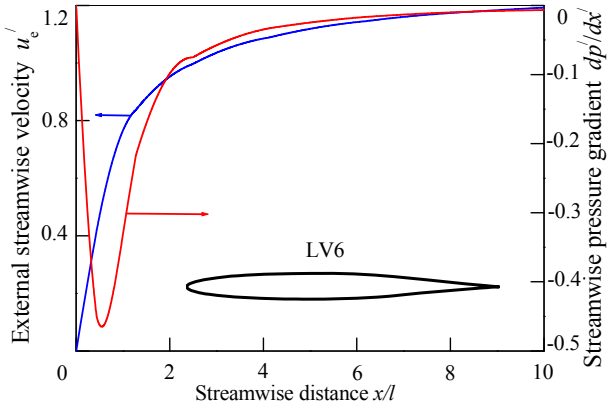

Fig. 4. Dimensionless external streamwise velocity and pressure gradient

In reality DBD-actuators generate both horizontal (parallel to a dielectric surface) and vertical (normal to the surface) components of the volumetric force. Theoretical estimations [12] show that the impact of the vertical force component directed to the solid surface on a boundary layer flow can be noticeable if this component is much greater than the horizontal one and is not uniform along the surface. But experiments demonstrate that the horizontal force in DBD exceeds essentially the vertical one [13]. Therefore the influence of the vertical volumetric force on a boundary layer flow is not taken into account.

It is evident also that a variation of static pressure along a wing chord will influence on discharge characteristics and, hence, on distributions of the volumetric force and energy input. But this effect is neglected in the current approximate consideration.

A possibility to use the usual boundary layer approximation in the considered case is proved in [14]. The boundary layer flow is determined by the velocity components u, v, w, the static pressure p, the air density ρ, the static enthalpy $h = c_p T$ which are governed by the following system of the equations and boundary conditions:

$$\frac{\partial(\rho u)}{\partial x} + \frac{\partial(\rho v)}{\partial y} + \frac{\partial(\rho w)}{\partial z} = 0 \qquad (2)$$

$$\rho u \frac{\partial u}{\partial x} + \rho v \frac{\partial u}{\partial y} + \rho w \frac{\partial u}{\partial z} = \frac{\partial}{\partial y}\left(\mu \frac{\partial u}{\partial y}\right) - \frac{dp}{dx} + F_x$$

$$\rho u \frac{\partial w}{\partial x} + \rho v \frac{\partial w}{\partial y} + \rho w \frac{\partial w}{\partial z} = \frac{\partial}{\partial y}\left(\mu \frac{\partial w}{\partial y}\right) + F_z$$

$$\rho u \frac{\partial h}{\partial x} + \rho v \frac{\partial h}{\partial y} + \rho w \frac{\partial h}{\partial z} = \frac{\partial}{\partial y}\left(\frac{\mu}{\mathrm{Pr}} \frac{\partial h}{\partial y}\right) + u \frac{dp}{dx} + Q + \mu\left[\left(\frac{\partial u}{\partial y}\right)^2 + \left(\frac{\partial w}{\partial y}\right)^2\right]$$

$$p = \rho R T$$

$$y = 0: \; u = v = w = \partial h / \partial y = 0$$
$$y = y_e: \; u = u_e, \; w = w_e, \; h = h_e$$

$$w_e = V_\infty \sin\chi$$
$$h_e = h_\infty + 0.5\left(V_\infty^2 - u_e^2 - w_e^2\right)$$

$$\mu(T) = 1.47 \cdot 10^{-6} \frac{T^{3/2}}{T + 114}$$
$$\gamma = 1.4, \; \mathrm{Pr} = 0.72$$

Here F_x, F_z and Q are the spatial distributions of the time averaged components of horizontal volumetric force $F_\parallel$ and total Joule dissipation generated in every actuator and

determined in analytical form below. It is evident that F_x=0, F_z=$F_{\|}$ in variant *1* of actuators arrangement (see Fig. 3, *a*) and $F_x = -F_{\|} \sin\psi$, $F_z = F_{\|} \cos\psi$ for variant *2* (Fig. 3, *b*).

The relation of the total (space integrated and time averaged) body force $\langle F \rangle$ per unit length of the exposed electrode (N/m) to total Joule dissipation $\langle J \rangle$ (W/m) generated by every DBD-actuator determines its energy efficiency $E = \langle F \rangle / \langle J \rangle$. This relation has a physical sense of reverse average drift velocity of charge carriers and depends on actuator geometry, gas pressure, and other physical parameters [15]. Numerical modeling of multiple DBD-actuator at a given above air static pressure resulted in $E = 2.5 \cdot 10^{-4}$ s/m [16]. This value of energy efficiency is used in the present calculations.

Simple estimations of actuators impact on boundary layer flow have been obtained at the assumption of uniform force and heat input distributions in spanwise direction, i. e. $\partial/\partial z \equiv 0$. Supposing that every actuator creates total force $\langle F \rangle$ and the distance between actuators (spatial period) equals z_0, the span-uniform volumetric force and heat input distributions are taken as

$$F_u(y) = \langle F \rangle \frac{1}{z_0 y_{0F}} \frac{2}{\sqrt{\pi}} \exp\left[-\left(\frac{y}{y_{0F}} \right)^2 \right] \qquad (3)$$

$$Q_u(y) = \frac{\langle F \rangle}{E} \frac{1}{z_0 y_{0Q}} \frac{2}{\sqrt{\pi}} \exp\left[-\left(\frac{y}{y_{0Q}} \right)^2 \right]$$

Here y_{0F} and y_{0Q} are the characteristic sizes of the force and heat input distributions perpendicular to a wing surface.

First of all note that two competing effects on cross-flow appear in the considered case. The volumetric force impact in variant *1* results in an increase in *w*-component and according to (1) a decrease in cross-flow velocity. But a gas heating owing to Joule dissipation at a given streamwise distribution of static pressure results in a decrease in gas density and, as a consequence, an increase in *u*-component of gas velocity [14]. According to (1), this thermal impact leads to an increase in cross-flow velocity.

The results of this competition of force and heat impact are illustrated in Fig. 5 where the cross-flow velocity distributions defined by the first expression (1) are presented in the cross-section $x/l = 0.5$ where the absolute value of the streamwise pressure gradient is close to maximal (see Fig. 4). The spanwise uniform impacts are calculated for both variants of the actuators arrangement at the following parameters: the total force generated by every actuator $\langle F \rangle = 0.02$ N/m, the energy efficiency $E = 2.5 \cdot 10^{-4}$ s/m, the spatial period of actuators in series $z_0 = 5$ mm, the characteristic vertical sizes are $y_{0F} = 0.2$ mm for force source and $y_{0Q} = 0.15$ mm for heat input source.

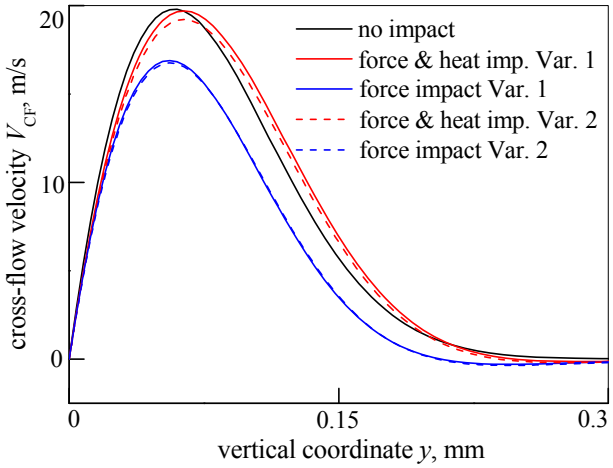

Fig. 5. Cross-flow velocity in the cross-section x/l=0.5

One can see that pure force impact in both variants results in a decrease of the cross-flow velocity but the unfavorable effect of gas heating appreciably weakens this effect. A decrease of the cross-flow velocity is somewhat greater in variant *2* in the case of both force and heat impact.

To estimate the influence of spanwise non-uniformity of force and heat impact the following analytic expression for volumetric force sources presenting in (2) was taken:

$$F_{\|}(s,y) = \frac{40 \langle F \rangle}{\sqrt{\pi} s_{0F} y_{0F}} f_s(s) f_y(y) \qquad (4)$$

$$f_s(s) = \frac{s}{s_{0F}} \left(1 - \frac{s}{s_{0F}} \right)^3$$

$$f_y(y) = \exp\left[-\left(\frac{y}{y_{0F}} \right)^2 \right]$$

$$< F >= \int_0^{s_0} ds \int_0^{\infty} F_{\|}(s, y) dy$$

Here s is the distance along a wing surface ($s = z$ in variant *1*), s_{0F} and y_{0F} are horizontal and characteristic vertical sizes of the force source. The heat release source $Q(s, y)$ is taken in similar form with replacing $<F>$ by $<F>/E$ and differing characteristic sizes s_{0Q} and y_{0Q}.

Numerical solution of the system (2) at given distributions of flow parameters on the external boundary y_e according to Fig. 4 with taking into account a flow periodicity in z-direction has been executed with the use of the expansion of all dependent variables and volumetric sources (4) in finite Fourier series and subsequent solution of the resulting 2D equation systems.

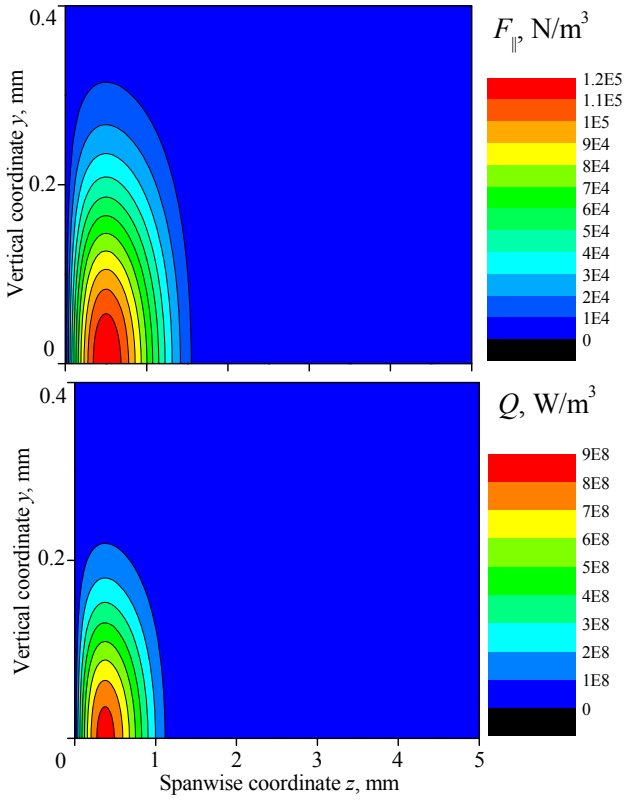

Fig. 6. Spatial distributions of volumetric force and heat release sources

The force and heat input distributions (4) for $<F> = 0.02$ N/m, $E = 2.5 \cdot 10^{-4}$ s/m, $z_0 = 5$ mm, $s_{0F} = 2$ mm, $y_{0F} = 0.2$ mm, $s_{0Q} = 1.5$ mm, $y_{0Q} = 0.15$ mm are presented in Fig. 6. Note, that the force distribution shown in upper Fig. 6 qualitatively corresponds to results of both experiments [13] and numerical modeling [16]. Maximal value of the force distribution in Fig. 6 is close to that used in numerical modeling [11] and up to order less than in [17].

The boundary layer flow becomes spatially modulated along a wing span because of non-uniform force and heat impact of actuators (4). For example, the cross-flow velocity and the gas temperature distributions in the streamwise cross-section $x/l = 1$ for variant *1* (Fig. 3, *a*) are presented in Fig. 7.

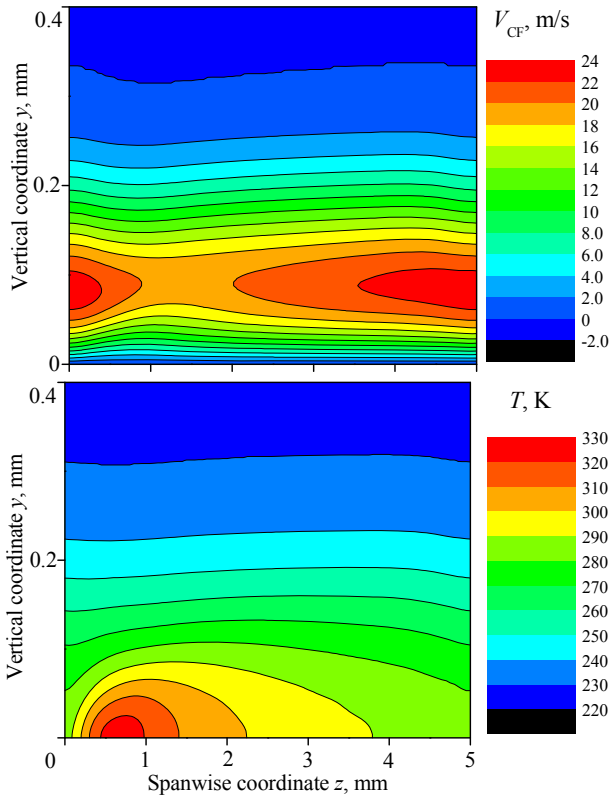

Fig. 7. Distributions of the cross-flow velocity and the gas temperature in the cross-section $x/l = 1$

Nevertheless the influence of the force and heat impact non-uniformity on the span-averaged cross-flow velocity (defined as zero term in Fourier series) is not significant as it is shown below. Figure 8 demonstrates the streamwise distributions of maximal values of the cross-flow velocity for the cases presented in Fig. 5. The black solid curve corresponds to usual boundary layer without impact of actuators. The blue solid curve corresponds to uniform pure force impact (3) in variant *1* of actuators arrangement, the blue dashed curve is the same in variant *2*. The red solid and dashed

curves correspond to both force and heat impact in variant *1* and 2, respectively. Finally, the dash-dotted red curve represents the result of non-uniform force and heat impact (4) in variant *1*.

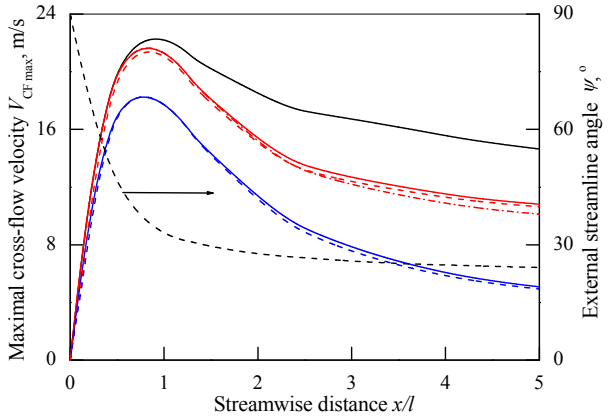

Fig. 8. Streamwise distributions of the maximal cross-flow velocity and the external streamline angle

One can see that the effect of spanwise uniform both pure force impact and combined force and heat impact in variant *2* is greater as compared to variant *1* but the difference between these variants is very insignificant. One can suppose that the advantage of variant *1* consisting in simultaneous deceleration of *u*-component and acceleration of *w*-component of the flow velocity is realized inside too short part of the boundary layer where the angle ψ are large enough. In turn the effect of only *w*-component acceleration in variant *1* at the same total force $F_{\|}$ is accumulated beginning from the critical line and appears downstream resulting in almost similar attenuation of V_{CF}.

Finally Fig. 8 demonstrates that non-uniformity of force and heat impact in spanwise direction influences weakly on span-averaged maximum of the cross-flow velocity.

3 Cross-flow stability calculations

The influence of plasma actuators on boundary layer stability is estimated in the framework of the linear stability equation system of Dunn-Lin [18]. The spanwise spatial modulation of the boundary layer flow is not taken into account in the present simplified consideration. It means that only zero terms of Fourier expansions of undisturbed flow functions are used in the stability analysis.

Only steady cross-flow-type disturbances are considered. The well-known e^N-method is used to estimate the position of laminar-turbulent transition [2]. So the disturbances of all flow functions q and the N factor are defined as follows:

$$q = q^*(y)\exp(-\alpha_i x)\exp[i(\alpha_r x + \beta z)] \quad (5)$$

$$N(x) = -\int_{x_0}^{x} \alpha_i dx$$

Here q^* is the complex eigenfunction, $\alpha = \alpha_r + i\alpha_i$ is the complex eigenvalue, α_r and β represent the wavenumber components in *x*- and *z*-directions, α_i represents increment of spatial growth ($\alpha_i < 0$) or decrement of decay ($\alpha_i > 0$) of disturbances, x_0 is the initial coordinate where α_i obtains negative value, i.e. the boundary layer flow becomes unstable.

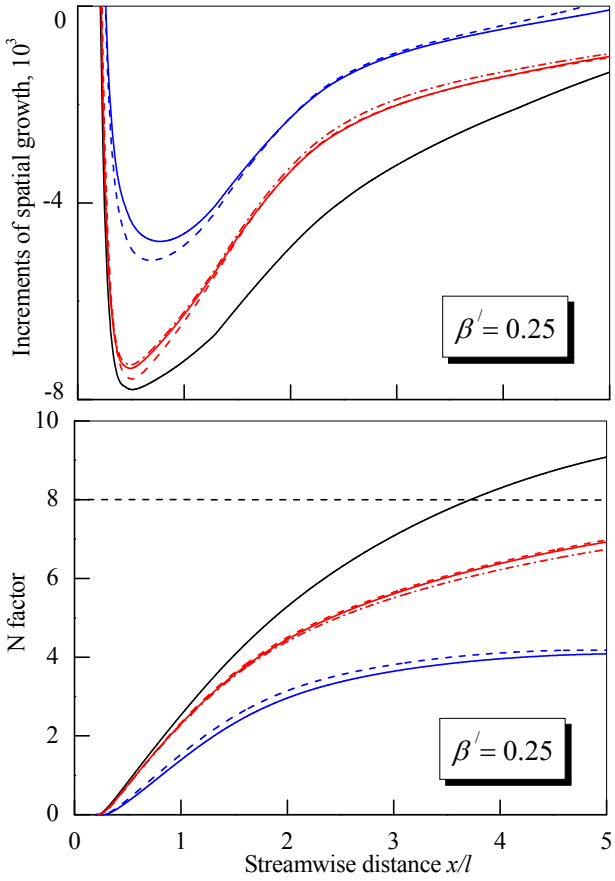

Fig. 9. Streamwise distributions of non-dimensional increments of spatial growth and *N* factor for $\beta' = 0.25$

The so-called fixed β strategy [2] is used for *N* factor computation. That is the streamwise distributions of the eigenvalue α and the *N*

factor are calculated according to (5) for a set of fixed spanwise wavenumbers β.

The calculated distributions of the dimensionless increments of spatial growth $\alpha' = \alpha l \mathrm{Re}^{-1/2}$ and N factors in streamwise direction for several dimensionless spanwise wavenumbers $\beta' = \beta l \mathrm{Re}^{-1/2}$ are presented in Figs. 9-11. Designations of the curves are similar to Fig. 8.

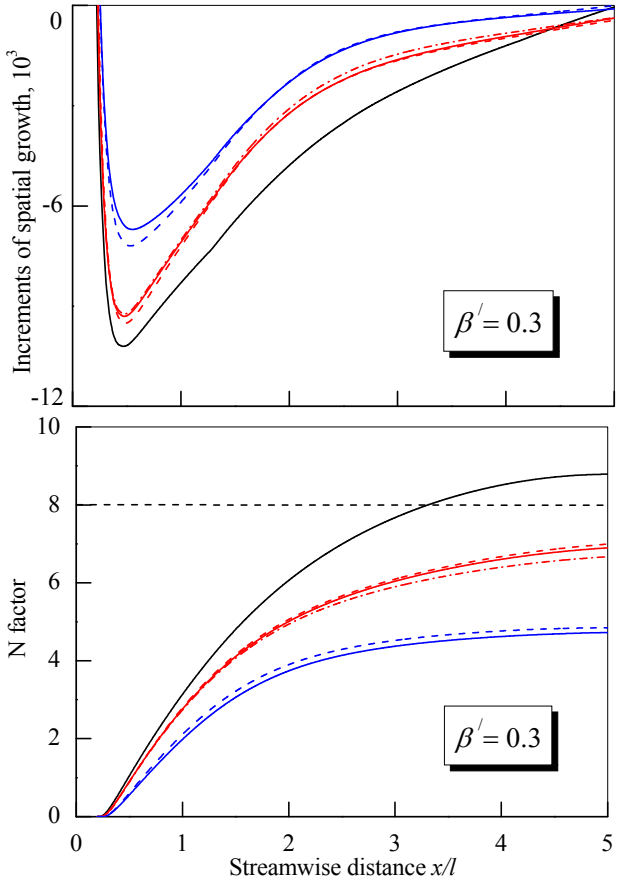

Fig. 10. Streamwise distributions of non-dimensional increments of spatial growth and N factor for $\beta' = 0.3$

The e^N-method implies that laminar-turbulent transition occurs when N factor calculated according to (5) for any spanwise wavenumber reaches some predefined value N_T. The position of the cross-flow induced transition is estimated by $N_T = 8\text{-}10$ for the fixed β strategy used here [2]. Using the lower value $N_T = 8$, one can see in Fig. 9 that transition can occur in boundary layer without impact of actuators at the distance $x/l = 3.3$ for $\beta' = 0.3$. The steady disturbances with spanwise wavenumbers $\beta' > 0.35$ are nonhazardous according to Fig. 11.

The results presented in Figs. 9-11 show that a spanwise non-uniformity of force and heat sources influences weakly on increments of spatial growth of steady cross-flow disturbances. The difference between two considered variants of actuators arrangement remains insignificant too. The harmful influence of heat input on boundary layer stability is evident.

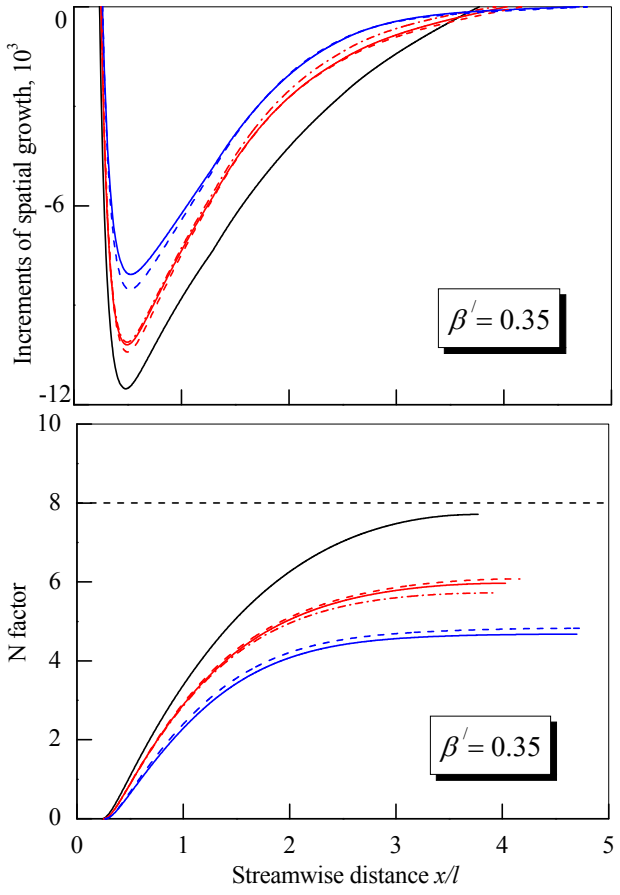

Fig. 11. Streamwise distributions of non-dimensional increments of spatial growth and N factor for $\beta' = 0.35$

Nevertheless the force and heat impact in simpler variant *1* permits to remove laminar-turbulent transition caused by the cross-flow-type instability in the considered concrete case. The average densities of the volumetric force and the consumed electric power per unit area of a wing surface are estimated as $F_S = \langle F \rangle / z_0 = 4$ N/m^2, $J_S = F_S / E = 16$ kW/m^2, respectively. This power about twice as large as compared to the mechanical power required to overcome the turbulent skin friction on a wing in cruise flight. But DBD-actuators required to remove a laminar-turbulent transition caused by

the cross-flow-type instability may cover only a few percent of a wing surface near a leading edge. Therefore a significant savings in mechanical power can be obtained due to laminarization about a half of a wing surface (approximately up to static pressure minimum) if the transition induced by Tollmien–Schlichting instability will be suppressed, for example, owing to appropriate favorable streamwise pressure gradient.

4 Conclusions

- The difference between two considered variants of actuators arrangement is insignificant.
- The influence of the spanwise non-uniformity of force and heat impact of plasma actuators on cross-flow instability is insignificant.
- Both the boundary layer flow and the cross-flow stability characteristics are very sensitive to volumetric heat input and, hence, to energy efficiency of plasma actuators. It demands thorough optimization of multiple DBD-actuators.
- The average density of the volumetric force per unit area of a wing surface of a few N/m^2 seems to be sufficient for delaying laminar-turbulent transition caused by cross-flow-type instability at cruise flight conditions.

Acknowledgments

This work was supported by Russian Foundation for Basic Research (Project # 12-01-00086).

References

[1] Abbas A, de Vicente J and Valero E. Aerodynamic technologies to improve aircraft performance. *Aerospace Sci. & Technol.*, Vol. 28, pp 100–132, 2013.

[2] Arnal D and Casalis G. Laminar-turbulent transition prediction in three-dimensional flows. *Prog. Aerospace Sci.*, Vol. 36, pp 173–191, 2000.

[3] Chernyshev S, Kiselev A and Kuryachii A. Laminar flow control research at TsAGI: Past and present. *Prog. Aerospace Sci*, Vol. 47, pp 169-185, 2011.

[4] Moreau T. Airflow control by non-thermal plasma actuators. *J. Phys. D: Appl. Phys.,* Vol. 40, pp 605-636, 2007.

[5] Corke T, Enloe C and Wilkinson S. Dielectric barrier discharge plasma actuators for flow control. *Annu. Rev. Fluid Mech.*, Vol. 42, pp 505-529, 2010.

[6] Wang J, Choi K-S, Feng L, Jukes T and Whalley R. Recent developments in DBD plasma flow control. *Prog. Aerospace Sci*., Vol. 62, pp 52–78, 2013.

[7] Mack L. On the stability of the boundary layer on a transonic swept wing. *AIAA Paper*, No. 264, pp 1-11, 1979.

[8] Kuryachii A, Rusyanov D, Chernyshev S and Skvortsov V. About increase of efficiency of plasma multi-actuator system for boundary layer control. *TsAGI Sci. Journal*., Vol. 44, No. 3, pp 305-326, 2013.

[9] Benard N, Jolibois J, Mizuno A and Moreau E. Innovative three-electrode design for definition of multiple dielectric barrier discharge actuators. *Proc. of 2009 Electrostatic joint Conference*, Boston, paper # P1.17, pp 1-8, 2009.

[10] Chernyshev S, Kuryachii A, Manuilovich S, Rusyanov D and Skvortsov V. Attenuation of cross-flow-type instability in compressible boundary layer by means of plasma actuators. *AIAA Paper*, No. 321, pp 1-16, 2013.

[11] Fedorov A, Krivtsov V, Soloviev V and Soudakov V. Modeling of aerodynamic forcing induced by surface dielectric barrier discharge. *AIAA Paper*, No. 158, pp 1-13, 2011.

[12] Kuryachii A. Effect of a space-time source structure simulating a dielectric barrier discharge on the laminar boundary layer. *Fluid Dynamics*, Vol. 41, No. 3, pp 366-374, 2006.

[13] Benard N, Debien A. and Moreau E. Time-dependent volume force produced by a non-thermal plasma actuator from experimental velocity field. *J. Phys. D: Appl. Phys.,* Vol. 46, p 245201, 2013.

[14] Kuryachii A, and Manuilovich S. Attenuation of cross-flow-type instability in a 3D boundary layer due to volumetric force impact. *TsAGI Sci. Journal*, Vol. 42, No. 3, pp 345-360, 2011.

[15] Kuryachii A, Rusyanov D and Skvortsov V. Modeling of dielectric barrier discharge actuators at various gas pressures and estimation of their influence on shear flows. *TsAGI Sci. Journal*, Vol. 42, No.2, pp 227-243, 2011.

[16] Chernyshev S, Kuryachii A, Manuilovich S, Rusyanov D and Skvortsov V. On a possibility of laminar flow control on a swept wing by means of plasma actuators. *CD-ROM Proceedings of the 5th European Conference for Aeronautics and Space Sciences* (*EUCAS 2013*), Munich, ISBN: 978-84-941531-0-5, pp 1-12, 2013.

[17] Likhanskii A, Shneider M, Opaits D, Macheret S and Miles R. Limitations of the DBD effects on the external flow // *AIAA Paper*, No. 470, pp. 1-13, 2010.

[18] Dunn D and Lin C. The stability of the laminar boundary layer in a compressible fluid for the case of three-dimensional disturbances. *J. Aeronautical Sci.,* Vol. 19, pp 491–502, 1952.

Contact Author Email Address

mailto: aleksandr.kuryachiy@tsagi.ru

Copyright Statement